Premier Journal of Engineering and Applied Sciences
Publication of Nigerian Society of Engineers, Ibadan Branch
P J E A S
Vol. 1, No. 2, 2020

# Grating Lobes Suppression in Linear Arrays of Resonant Half-wave Dipoles

**T. Christiana Erinosho[a*], S. Adeniyi Adekola[a,b], K. Akinwale Amusa[a]**

[a]Department of Electrical and Electronics Engineering, Federal University of Agriculture, Abeokuta, Nigeria
[b]Department of Electrical and Electronics Engineering, Federal University of Otuoke, Otuoke, Nigeria

***Corresponding Author:*** *toluerinosho@gmail.com*

**ARTICLE INFO**

*Received: November, 2019*
*Accepted: March, 2020*
*Published: April, 2020*

*Keywords:*
Grating lobes
Array factor
Method of moment
Inter-element spacing

**ABSTRACT**

*This paper investigates how undesirable grating lobes can be suppressed from the visible range of patterns radiated by a linear array of identical resonant dipoles. Using Method of Moments (MoM) approach, the far-zone electric field intensity due to the primary array element is determined, and following the pattern multiplication principle, a product of the elemental pattern and the array factor provides an expression for the total field radiated by the linear array, in terms of design parameters, including inter-element spacing. It is found from computational results that the upper bound for inter-element separation assumes values of* 0.45 λ and 0.41 λ *for the suppression of grating lobes in the cases of broadside and ordinary end-fire linear arrays, respectively. Results of several computations reveal certain interesting features. An expression to determine the number of grating lobes in both the array factor and in the corresponding total electric field pattern radiated for the linear arrays of dipole is easily obtained and presented. With this result, grating lobes suppression in linear array is realizable by careful choice of inter-element separation and its integral multiples.*

## 1. INTRODUCTION

A multi-element antenna called an antenna array produces better radiation characteristics than a single element antenna (Erinsho *et al.*, 2017). The antenna type, geometrical arrangement of elements of the array and the choice of excitation, combined to determine the overall radiation pattern of the array antenna. However, in the design of such array of antennas, especially those for broadcasting applications, grating lobe, which is almost of equal magnitude as the main lobe but radiates in an undesired direction, must be adequately suppressed. This is because the total power radiated by the elements of the array is shared between the main lobe and the grating lobes thereby leading to a waste of electromagnetic energy and reduction in power efficiency of the antenna (Vosoogh and Kildal, 2016). Additionally, these spurious signals constitute a health hazard to the personnel working in the vicinity of the antennas and increase the level of electromagnetic interference in the air space.

Several solutions and techniques have been proposed for the suppression of grating lobes in the literature. The list includes grating lobes suppression via discontinuity of the periodicity of the array elements (Wang

*et al.*, 2008), the use of Tabu-search algorithm (Merad *et al.*, 2008), replacement of individual elements in a linear array with a pair of elements called a discrete dipole element (Chakravorty and Mandal, 2016) and a host of other methods that can be found in the literature where similar problem is addressed (Wang *et al.*, 2018; Oliveri and Massa, 2011; Sharma and Fiete, 1988). However, validity of proposed solutions in those previous studies are premised on the assumption that the inter-element spacing between array elements is not more than half-wavelength (Suarez *et al.*, 2012; Alshammary *et al.*, 1981; Amlaner, 1979). How close or far from half-wavelength the spacing will be is left for individual choice.

In this study, an approach for the determination of the optimum inter-element spacing for grating lobe suppression in a linear array of resonant dipoles is proposed. In addition, a general expression to quantify the possible number of grating lobes that is in a typical linear array of antenna of a given geometrical configuration is provided. Sparse arrays produce more grating lobes compared with uniformly spaced arrays (Wang *et al.*, 2018; Oliveri and Massa, 2011). Therefore, broadside and ordinary end-fire linear arrays of dipoles are investigated in such a manner that the undesirable grating lobe is completely suppressed within the visible range. Since directivity is a function of radiation intensity, which is directly proportional to pattern radiated by an antenna, investigated also is the effect of the number of elements on the directivity and side-lobe level in the array pattern. This is considered pertinent as there is always a trade-off between directivity and side-lobe level suppression in wireless communication systems. MoM is employed as the numerical tool while analyzing the problem of the single dipole element using the entire basis function in the expansion of the unknown current, which constitutes the radiation source, in the antenna structure.

## 2. METHODOLOGY

The geometry of an elemental dipole adopted in this work is a half-wave dipole antenna excited by a 1-Volt delta gap source as shown in Figure 1.

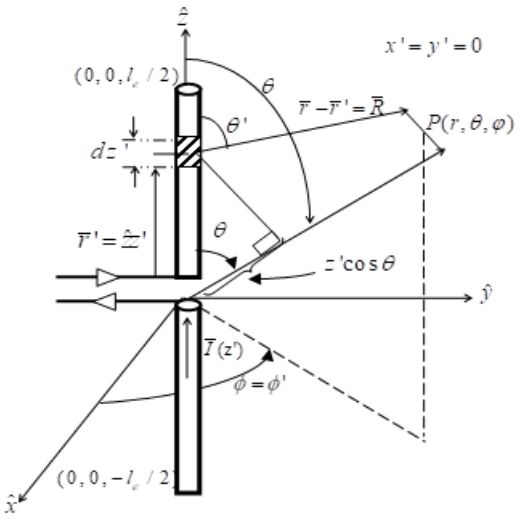


**Fig. 1: Geometrical representation of half-wave dipole fed by a delta-gap source**

For MoM to be used in the numerical analysis of a wire antenna and in an attempt to develop a generalized formulation for the electromagnetic field's expressions, it is assumed that the dipole is electrically thin and perfectly conducting. The feed-point impedance $z_{in}$ of a dipole is highly sensitive to its electrical length and the location of the feed-point. Hence, dipole performs optimally over a narrow bandwidth beyond which

its impedance becomes a poor match for the transmitter and receiver. The feed-point impedance, $z_{in}$ can be generally expressed as

$$Z_{in} = R_{in} + jX_d \quad (1)$$

provided $(R_{in}, X_d)$ are the input resistance and reactance of the dipole, respectively. It is a known fact that the diameter of the wire determines the value of the reactance, $X_d$. However, for a half-wave dipole, its radiation resistance is far greater than the impedance of the transmission line ( $R_d \geq Z_{in}$), which is also much larger than the input resistance, $R_{in}$ of the wire, hence its efficiency approaches 100%. In other to remove the reactance in a dipole for the transmission line, its length is reduced by an adjustment factor, $q$ whose value depends on the diameter $d$, of the wire. For a thin wire, having diameter, $d = 10^{-5}\lambda$, $q = 0.98$, whereas for a thick wire, $d = 0.008\lambda$, $q = 0.94$ (Stutzman, 1981). Thus, dipole antennas made from wires with these diameters are resonant owing to the fact that values of their reactance are zero and maximum power transferred is guaranteed in such situation.

Based on the foregoing, a rule of thumb to obtain the resonant length $l_e$ of a typical wire antenna of physical length $l_p$ is by multiplying $l_p$ with the adjustment factor. That is

$$l_e = q \times l_p \quad (2)$$

For a half-wave dipole, its electrical length is given as

$$l_e = q \times 0.5\lambda \quad (3)$$

which yields a value of $l_e = 0.49\lambda$ for a thin wire resonant dipole with the radius of the dipole, $a = 5\times10^{-6}\lambda$. This value is adopted as the electrical length of an elemental dipole in the analysis presented in this work.

### 2.1 Electromagnetic (EM) Fields Radiated by Half-wave Resonant Dipole

Since the dipole is assumed to be perfectly conducting and the incident field exists only at the antenna terminal (feed gap), it follows that the total electric field component that is tangential to the surface of the wire is identically equal to zero such that

$$\bar{E}_z^s = -\bar{E}_z^i \qquad \frac{-l}{2} \leq z \leq \frac{l}{2} \quad (4)$$

provided $\bar{E}_z^s$ is the radiated field due to the current $\bar{I}(z')$ resulting from the source field, $\bar{E}_z^i$.

Consider the wire from which the dipole is made to be of infinite conductivity and very thin wire, then without loss of generality, one may assume that the current flowing is confined to the surface of the wire and has a z-directed axial component only. Consequent of above assumptions, the associated magnetic vector potential admits the form expressible as

$$\bar{A}_z = \frac{\mu_0}{4\pi}\int_{-l/2}^{l/2} \bar{I}(z')\frac{e^{-j\beta_0 R}}{R}dz' \quad (5)$$

and the corresponding electric field radiated by the dipole at the observation point is written as

$$\bar{E}_z^s = -j\omega\mu_0\bar{A}_z \quad (6)$$

where $(\mu_0, \beta_0)$ are the permeability of free space and the wave number, respectively, and R is the distance from the source point to the field point P as depicted in the Figure 1.

Invoking appropriate far-field approximations and using (5) and (7) in (6), the θ-component of the electric field radiated by an elemental dipole assumes the form expressible as

$$E_\theta = \frac{j\omega\mu_0 e^{-j\beta_0 r}\sin\theta}{4\pi r}\int_{-l/2}^{+l/2} I(z')e^{j\beta_0 z'\cos\theta}dz' \tag{7}$$

The unknown current $I(z')$ present in the integral equation described by (7) is obtainable through the use of the MoM procedure when (7) is re-cast in a form expressible as

$$L(u) = h \tag{8}$$

where $L$ is an integro-differential linear operator, $u$ is the unknown quantity $I(z')$ and $h$ is the known source field. Application of MoM procedure allows the unknown function $I(z')$ in (7) to be rendered in terms of known basis function $g_m$ and unknown expansion coefficients, $I_n$ as

$$I(z') = \sum_{n=1}^{N} I_n g_m(z') \tag{9}$$

provided $I_n$ represents the unknown complex current coefficient of mode n on the element and $g_m(z')$ is the basis function defined globally as

$$g_m(z') = \cos\left[\frac{(2m-1)\pi z'}{l}\right] \tag{10}$$

Using a delta function as the testing function and applying Galerkin's method on the expansion function coupled with the use of suitable trigonometric identities, (7) assumes a form written as

$$E_\theta = \frac{j\omega\mu_0\ e^{-j\beta_0 r}\sin\theta}{4\pi r}\sum_{n=1}^{N} I_n\left(\left\{\left[\mathrm{sinc}(A^+)\right]+\left[\mathrm{sinc}(A^-)\right]\right\}\lambda/4\right) \tag{11}$$

where,

$$A^+ = \left(\frac{2(2m-1)\pi}{\lambda}+\beta_0\cos\theta\right)\frac{\lambda}{4} \tag{11a}$$

and

$$A^- = \left(\frac{2(2m-1)\pi}{\lambda}-\beta_0\cos\theta\right)\frac{\lambda}{4} \tag{11b}$$

The corresponding far zone magnetic field $H_\phi$ is obtained as

$$H_\phi = \frac{j\omega\mu_0\ e^{-j\beta_0 r}\sin\theta}{4\pi r\ \eta_0}\sum_{n=1}^{N} I_n\left(\left\{\left[\mathrm{sinc}(A^+)\right]+\left[\mathrm{sinc}(A^-)\right]\right\}\lambda/4\right) \tag{12}$$

where $\eta_o$ is the intrinsic impedance of free-space. The normalized electric field radiated by the dipole has been obtained elsewhere (Erinosho et al., 2017) as

$$E_n(\theta) = \sin\theta \tag{13}$$

### 2.2 Total Electric Field Radiated by Array of dipoles

Depicted in Figure 2 is an N-element array of identical dipoles that is positioned along the z-axis. Current flowing in each of the array elements symbolized by $I(z')$ is assumed equal for all elements of the array and flow along the z-axis. Hence, the array is said to be collinear.

A uniformly spaced distribution is assumed between the elements such that the total field radiated by the array of dipoles is obtained by pattern multiplication theorem, expressible in the form stated as

$$E_t(\theta,\varphi) = E_n(\theta,\varphi) \times |AF_n(\theta,\varphi)| \tag{14}$$

provided $E_n(\theta,\varphi)$, $|AF_n(\theta,\varphi)|$ are the normalized field pattern of an elemental dipole and normalized array factor, respectively. The normalized array factor is a function of the geometrical configuration of the array and respective excitation phase $\beta$, expressed as

$$AF_n(\theta,\varphi) = \left|\frac{\sin(0.5N\varphi)}{N\sin(0.5\varphi)}\right| \tag{15}$$

where

$$\varphi = kd_z\cos\theta + \beta \tag{15a}$$

provided $N$ is the number of elements in the array; β is the progressive phase shift between elements; θ is the elevation angle; $k = 2\pi/\lambda$ is the wavenumber and $d_z$ represents the inter-element spacing between array elements.

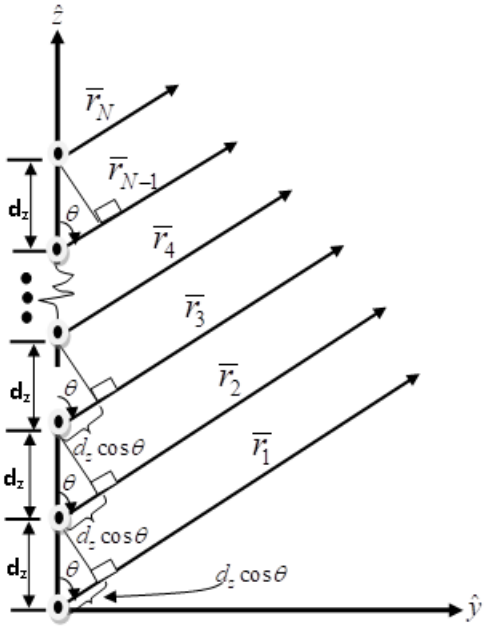


**Fig. 2: Geometry of an N-element collinear array of dipoles**

### 2.2.1 Broadside Arrangement of Array Elements

Here, the direction of the maximum radiation, $\theta_{max} = 90^0$. It follows that (15) is maximum at $\varphi = 0$, hence $\beta = 0$, with the corresponding normalized array factor obtained from (15) as

$$AF_n(\theta,\varphi)_{\theta=90^0} = \left|\frac{\sin(0.5N\varphi)}{N\sin(0.5\varphi)}\right| \tag{16}$$

and the corresponding normalized total field obtained from (14) as

$$(E(\theta,\varphi)_t)_n = \sin\theta\left|\frac{\sin(0.5N\varphi)}{N\sin(0.5\varphi)}\right| \tag{17}$$

where use has been made of (13) and (16) to arrive at (17).

### 2.2.2 End-fire Arrangement of Array Elements

This type of array has its maximum radiation along the axis of the array. Hence, for the array depicted in Figure 2, $\theta_{max} = 0^0$ *or* $180^0$. Application of this condition in (15) yields

$$AF_n(\theta,\varphi)_{\theta=0^0 or 180^0} = \left|\frac{\frac{1}{N}\sin(0.5Nkd_z(\cos\theta \text{ m} 1))}{\sin(0.5kd_z(\cos\theta \text{ m} 1))}\right| \tag{18}$$

from which the normalized total electric field of ordinary end-fire arrangement is obtained from (14) upon invocations of (13) and (17) as

$$(E(\theta,\varphi)_t)_n = \sin\theta\left|\frac{\frac{1}{N}\sin(0.5Nkd_z(\cos\theta \text{ m} 1))}{\sin(0.5kd_z(\cos\theta \text{ m} 1))}\right| \tag{19}$$

Presented and discussed in what follows are the numerical results of the array factor and the corresponding field patterns obtained at varying values of inter-element spacing, $d_z$. It worth mentioning that result obtained elsewhere (Erinosho *et al.*, 2017) is as guide on the choice of values of $d_z$ utilized in the investigation.

## 3. RESULTS AND DISCUSSION

In the computer simulations of the array of dipoles, use is made of MATLAB software. The results are presented in two modules: first is the array factor patterns computed using (16) and the corresponding electric field patterns for the broadside array, as computed from (17). Second, the array factor patterns computed from (18) and the corresponding electric field patterns for the ordinary end-fire array, as computed from (19) are displayed. The strategy employed for both array arrangements is to fix the number of elements, N, at 16, frequency, *f*, at 1200 MHz (GSM band) while computing patterns of array factor and field radiated, at different values of the inter-element spacing, $d_z$. Details of results computed are presented in what follows starting with the broadside array.

### 3.1 Broadside Case

Figures 3(a) – 3(d) depict responses of the array to increasing inter-element spacing. As expected, the directivity of the dipole array increases with inter-element separations, though, with generation of more side lobes. The patterns show that the optimum inter-element spacing, $d_{max}$ for broadside arrangement is 0.45 λ as portrayed in Figure 3(a). Beyond this value of inter-element separation, grating lobes begin to occur in the visible range of the pattern. These features are displayed in figures 3(b) – 3(d). It is observed that the number of Grating Lobes (GLs) appearing in the patterns when the spacing is an integral multiple of $d_{max}$ = 0.45 λ, follows a definite pattern. This is illustrated in Table 1.

**Table 1**: Analysis of GL in the patterns of the array factor and field radiated by broadside linear array of dipoles

| Values of $d_z$ (λ) | Equivalent value of $d_z$ in terms of $md_{max}$ | Number of GL in the array factor patterns *2(m-1)* | Number of GL in the Electric field patterns *2(m-1)* |
|---|---|---|---|
| 0.45 | $1\,d_{max}$ | 0 | 0 |
| 0.90 | $2\,d_{max}$ | 2 | 2 |
| 1.35 | $3\,d_{max}$ | 4 | 4 |
| 1.80 | $4\,d_{max}$ | 6 | 6 |

It can thus be inferred that in a broadside linear array of N-elements, having its fundamental maximum inter-element separation denoted as $d_{max}$, if the spacing between array elements is $md_{max}$, then the number of GLs appearing in the visible range of both patterns of the array factor and field radiated is given by $2(m-1)$, provided *m* is a positive integer.

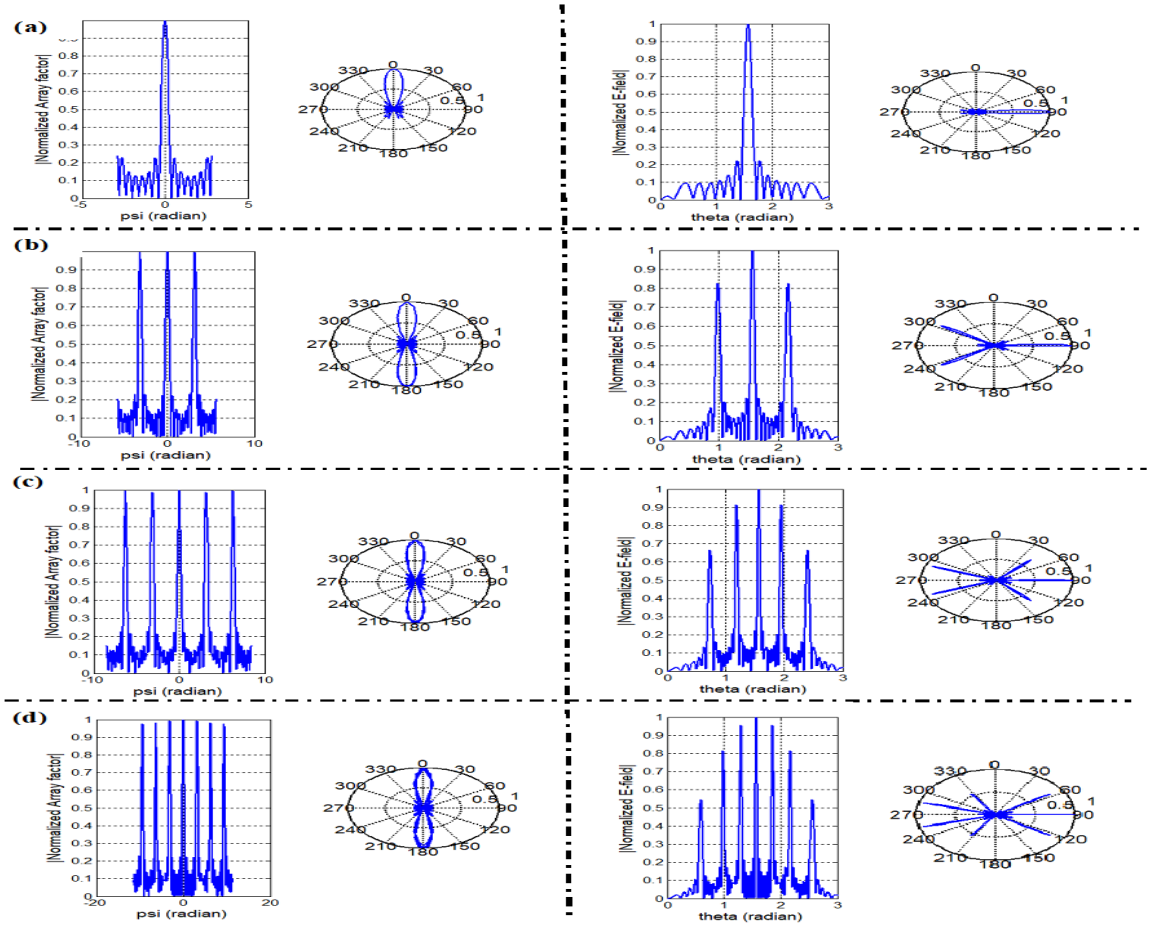


**Fig. 3: Normalized array factor and corresponding normalized total electric field patterns for broadside array of resonant half-wave dipole when N=16, f =1.2 GHz (a) $d_z$ = 0.45 λ (b) $d_z$ = 0.9 λ (c) $d_z$ = 1.35 λ (d) $d_z$ = 1.80 λ**

### *3.2 Ordinary End-fire Case*

Illustrated in Figures 4(a) – 4(d) are the array factor patterns together with the corresponding electric field patterns of an end-fire array, for $\theta = 180^0$. It is to be pointed that in Figure 4(a), $d_{\max}$ is identically equal to $0.41\lambda$ in order to accomplish complete grating lobe suppression for that end-fire array. As highlighted in Table 2, the number of grating lobes appearing in patterns of both array factor and field radiated also satisfy the expression $2(m-1)$ respectively, where m is a positive integer.

**Table 2:** Analysis of GL in the array factor and field patterns of an end-fire array of dipoles

| Values of $d_z$ ($\lambda$) | Equivalent value of $d_z$ in terms of $md_{\max}$ | Number of GLs in the array factor patterns *2(m-1)* | Number of GLs in the Electric field patterns *2(m-1)* |
|---|---|---|---|
| 0.41 | $1\,d_{\max}$ | 0 | 0 |
| 0.82 | $2\,d_{\max}$ | 1 | 2 |
| 1.23 | $3\,d_{\max}$ | 2 | 4 |
| 1.64 | $4\,d_{\max}$ | 3 | 6 |

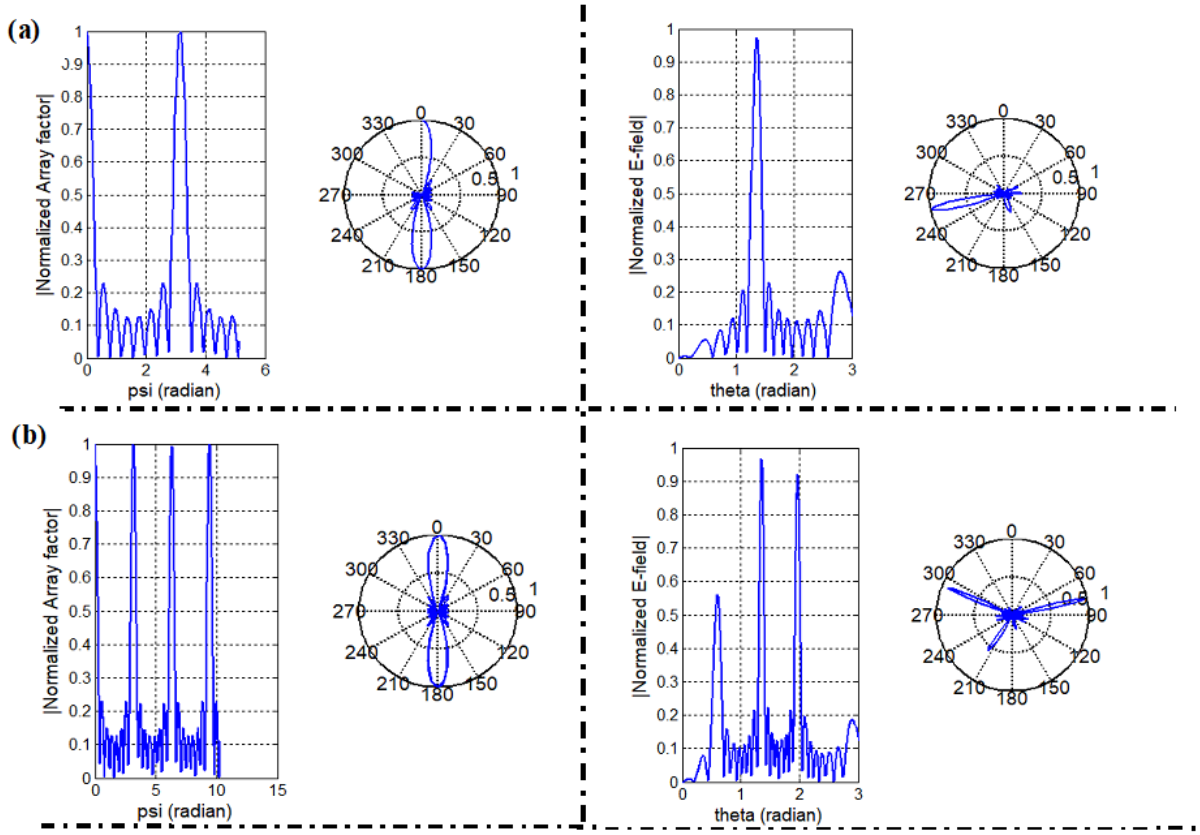

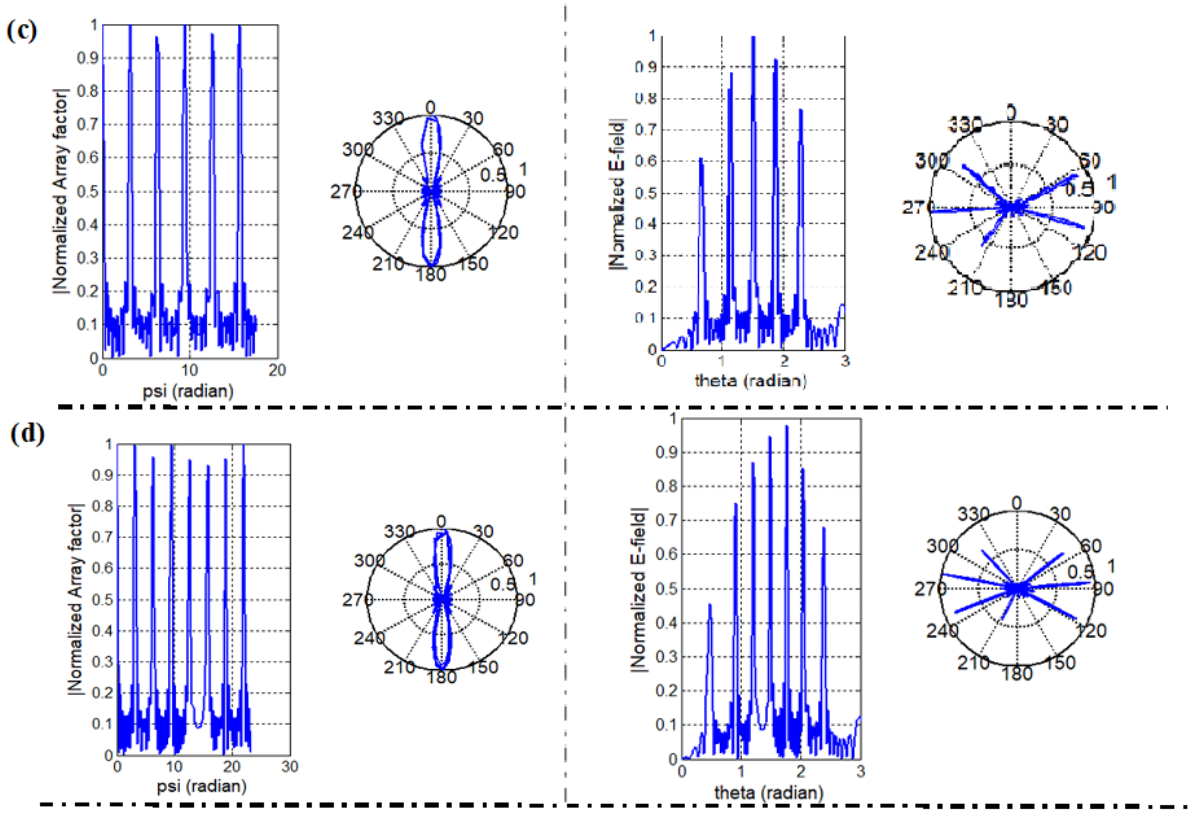


**Fig. 4: Normalized array factor and corresponding normalized total electric field patterns for ordinary end-fire array of resonant half-wave dipoles when N = 16, f = 1.2 GHz (a) $d_z = 0.41\ \lambda$ (b) $d_z = 0.82\ \lambda$ (c) $d_z = 1.23\ \lambda$ (d) $d_z = 1.64\ \lambda$**

## 4. CONCLUSION

It shown in this paper that the optimum inter-element separation designated as $d_{max}$ represents a veritable control measure for the removal of grating lobes from the visible range of patterns radiated by linear broadside and ordinary end-fire arrays of resonant dipoles. Indeed, optimum values of $d_{max}$ determined precisely here via several computations yield (0.45λ, 0.41λ) for the broadside and ordinary end-fire arrays, respectively. It is established here that if the inter-element spacing in linear array of resonant dipoles is given as $md_{max}$, where m is a positive integer and $d_{max}$ is the optimum inter-element separation, the number of grating lobes existing in the visible range of the array pattern is determined as $2(m-1)$, irrespective of whether the arrangement is broadside or ordinary end-fire. With this knowledge of method of predicting the number of grating lobes that are possible within the visible region of linear arrays, antenna design work will be greatly enhanced by careful selection of inter-element separations that will ensure non-appearance of un-desirable grating lobes.

**References**

Erinosho, T. C. and Adekola, S.A. (2017). Linear Array of Physically Resonant Half-Wave Dipoles. IEEE 3rd International Conference on Electro-Technology for National Development, Nigeria, 3: 86-95.

Vosoogh, A. and Kildal, P. (2016). Simple Formula for Aperture Efficiency Reduction due to Grating Lobes in Planar Arrays. IEEE Transactions on Antennas and Propagation, 1-6.

Wang, H., Fang, D. and Chow, Y. L. (2008). Grating Lobe Reduction in a Phased Array of Limited Scanning. IEEE Transactions on Antennas and Propagation, 56(6): 1581-1586.

Merad, L., Bendimerad, F. and Meriah, S. (2008). Design of Linear Antenna Arrays for Sidelobe Reduction using the Tabu Search Method. Int'l Arab Journal of Information Technology, 5(3): 219-222.

Chakravorty, P. and Mandal, D. (2016). Grating Lobe Suppression with Discrete Dipole Element Antenna Arrays. IEEE Antennas and Wireless Propagation Letters, 1-4.

Wang, Z., Wang, W., Zheng, Z. and Shao, H. (2018). Nested Array Sensor with Grating Lobe Suppression and Arbitrary Transmit-Receive Beampattern Synthesis. https://doi.org/10.1109/ACCESS.2018.2804486.

Oliveri, G. and Massa, A. (2011). Bayesian Compressive Sampling for Pattern Synthesis with Maximally Sparse Non-Uniform Linear Arrays. IEEE Transactions on Antennas and Propagation, 59(2): 467–481.

Wang, X., Wu, L., Li, M., Lu, S., Shang J. and Qiu, Q. (2016). Theoretical and Experimental Demonstration on Grating Lobes of Liquid Crystal of Array" International Journal of Optics, 7175809:1-6. z

Sharma, S.B. and Fiete, O.P. (1988). Gain Optimization with Suppressed Side Lobes and Grating Lobes in SBF Antenna. IETE Journal of Research, 34(6): 463-465.

Lu, B., Gong, S.X., Zhang, S., Guan, Y. and Ling, J. (2010). Optimum Spatial Arrangement of Array Elements for Suppression of Grating Lobes of Radar Cross Section. IEEE Antennas and Wireless Propagation Letters, 9: 114-117.

Suarez, S., Leon, G., Arrebola, M., Herran, L.F. and Las-Heras, F. (2012). Experimental Validation of Linear Aperiodic Array for Grating Lobe Suppression. Progress in Electromagnetics Research, 26: 193-203.

Alshammary, A., Weiss, S. and Nnorgi, S. (2017). Grating Lobe Suppression in Rotationally Tiled Arrays. 11th European Conference on Antenna and Propagation (EUCAP), IEEE Piscataway.

Stutzman, W.L. (1981). Antenna Theory and Design, John Wiley and Sons Inc., Canada.

Amlaner, C.J. (1979). "The Design of Antennas for use in Radio Telemetry", A Handbook on Biotelemetry and Radio Tracking: Proceedings of an International Conference on Telemetry and Radio Tracking in Biology and Medicine, Oxford.